# Application of the Godunov Method and Its Second-Order Extension to Cascade Flow Modeling

Shmuel Eidelman*
*Naval Postgraduate School, Monterey, California*
Phillip Colella†
*Lawrence Berkeley Laboratory, Berkeley, California*
and
Raymond P. Shreeve‡
*Naval Postgraduate School, Monterey, California*

**The Godunov method and a new second-order accurate extension of the method are used for the solution of two-dimensional Euler equations. Both numerical schemes are described in detail. Their performances in the subsonic, transonic, and supersonic flow regimes are first tested on the problem of flow in a channel with a circular arc bump. The methods are then applied to calculate the transonic flow through a supercritical compressor cascade designed by J. Sanz. For this case, the solution with the second-order extension of the Godunov method gives very good agreement with the design distribution of parameters given by Sanz.**

## Introduction

In recent years considerable attention has been given to numerical methods that use the analytical solution of the Riemann problem to calculate numerical fluxes at cell edges.[1,2]

The first method to employ the solution of the Riemann problem in its formulation was introduced in 1957 by Godunov[3] and has been widely used in the Soviet Union since then. The numerical simulation of a wide variety of gasdynamic, magnetogasdynamic, and two-phase flow problems using the Godunov method in one, two, and three dimensions has been reported in Russian publications.[3] Unfortunately, very limited information is usually given concerning the accuracy and convergence of the method in multidimensional cases. Until recently, experience with the Godunov method outside the USSR has been limited to one-dimensional shock wave problems.[4] It has been shown that the method, which is first-order accurate, solves nonlinear one-dimensional problems with the same or even better accuracy than many second-order accurate methods.[4]

Van Leer[1] was the first to extend the accuracy of the Godunov method to second order for solving gasdynamic problems in one space variable and in Lagrangian coordinates. These have since been reported in a number of investigations and further developments of higher-order extensions of Godunov's method.[2] In a comparative study by Woodward and Colella,[2] it was shown that the second-order extensions of the Godunov method gave superior results for supersonic flows with multiple-shock reflections. In view of these results it was decided to examine the performance of these methods in computing internal steady flowfields in comparison with the first-order accurate Godunov method. Godunov-type methods offer a distinct advantage in that they do not require the addition of artificial viscosity or smoothing, which is very appealing for aerodynamic engineering applications. The second-order extension of the Godunov method reported in this study is more accurate than the first-order one, but also does not require artificial viscosity or smoothing.

In the present work, results are reported for rotational subsonic, transonic, and supersonic inviscid internal flows obtained using a new code developed to implement the basic Godunov method and a second-order accurate extension of it. The overall purpose was to obtain accurate numerical simulations of transonic flows through cascades of turbomachine blading. The present paper provides descriptions of the implementation of the Godunov method, the second-order extension of the method, and results of applying the code to specific problems. Although the test cases presented are for steady-state flows, the goal eventually is to use the developed code for nonsteady problems. For this reason, an artificial means to accelerate convergence was not attempted.

## Governing Equations and Boundary Conditions

### Equations

The unsteady two-dimensional Euler equations can be written in conservation law form as

$$\frac{\partial U}{\partial t}+\frac{\partial F}{\partial X}+\frac{\partial G}{\partial Y}=0$$

where

$$U=\begin{bmatrix}\rho\\ \rho u\\ \rho v\\ e\end{bmatrix}\quad F=\begin{bmatrix}\rho u\\ p+\rho u^2\\ \rho uv\\ (e+p)u\end{bmatrix}\quad G=\begin{bmatrix}\rho v\\ \rho uv\\ p+\rho v^2\\ (e+p)v\end{bmatrix} \tag{1}$$

where $\rho$ is the density, $u$ and $v$ the velocity components in the $X$ and $Y$ coordinate directions, $p$ the pressure, and $\gamma$ the ratio of specific heats. The energy per unit of volume $e$ is defined by

$$e=\rho\left(\epsilon+\frac{u^2+v^2}{2}\right)$$

where $\epsilon=p/(\gamma-1)\rho$ is the internal energy. We look for the solution of the system of equations represented by Eq. (1) in

Presented as Paper 83-1941 at the AIAA Sixth Computational Fluid Dynamics Conference, Danvers, Mass., July 13-15, 1983; submitted July 25, 1983; revision received Dec. 20, 1983. This paper is declared a work of the U.S. Government and therefore is in the public domain.

*Adjunct Professor, Department of Aeronautics. Member AIAA.
†Staff Scientist, Computer Science and Mathematics Department.
‡Director, Turbopropulsion Laboratory. Member AIAA.

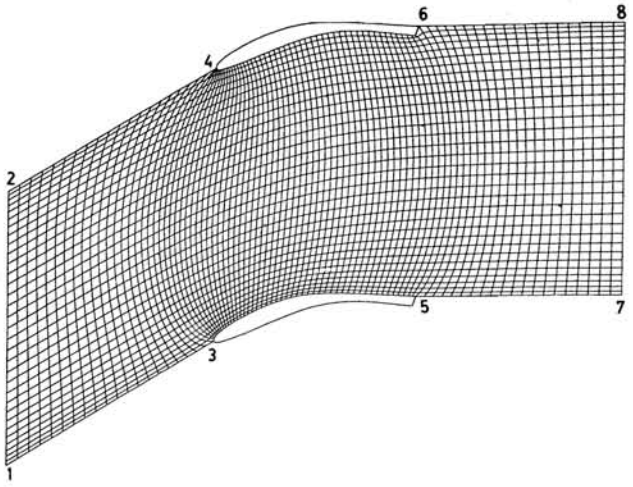


Fig. 1 Computational grid.

the computational domain shown in Fig. 1 for $t \to +\infty$ with the following conditions at the domain boundaries:

1) Inflow along segment 1-2.
2) Outflow along segment 7-8.
3) Solid wall along segments 3-5 and 4-6.
4) Cascade: periodicity between segments 1-3 and 2-4 and betweeen segments 5-7 and 6-8. Channel: solid wall along segments 1-7 and 2-8.

#### Inflow Conditions

The flow angle, the total enthalpy $H$, and entropy are specified and held constant at the upstream or inflow boundary. This leads to a unique definition of all flow parameters at the upstream boundary.

#### Outflow Conditions

If the outflow is subsonic at the downstream boundary, we define only the pressure $p_{\text{out}}$ and for all other flow parameters apply the continuation condition. That means that $u_{\text{out}}$, $v_{\text{out}}$, and $\rho_{\text{out}}$ are set equal to the values of $u$, $v$, and $\rho$ one point ahead of the downstream boundary.

If the outflow is supersonic, the continuation condition is applied to all parameters at the downstream boundary.

#### Solid-Wall Conditions

The solid-wall boundary condition appropriate for inviscid flow computations is that of zero mass flux through the surface. This condition is difficult to implement uniquely for the Euler equations. In the present work, two types of solid-wall conditions are implemented depending on the wall geometry. In regions where the wall curvature is smaller than 0.75, the condition on the surface is defined by solving the Riemann problem[3] between the point nearest to the wall in the domain of integration and its mirror image in the direction normal to the wall. The parameters of the "mirror" point are taken to be the same as those at the original point, but with the inverse sign taken for the velocity component normal to the wall. In regions where the wall curvature is larger than 0.75, the pressure at the wall is found from the conservation of momentum in the direction normal to the solid surface,[5] namely,

$$\partial_n p = \rho u_p^2 / R_s$$

where $n$ indicates the direction normal to the surface, $u_p$ the velocity parallel to the surface, and $R_s$ the radius of curvature of the surface. If we add to this the flow tangency condition, we have a uniquely defined boundary condition at the wall.

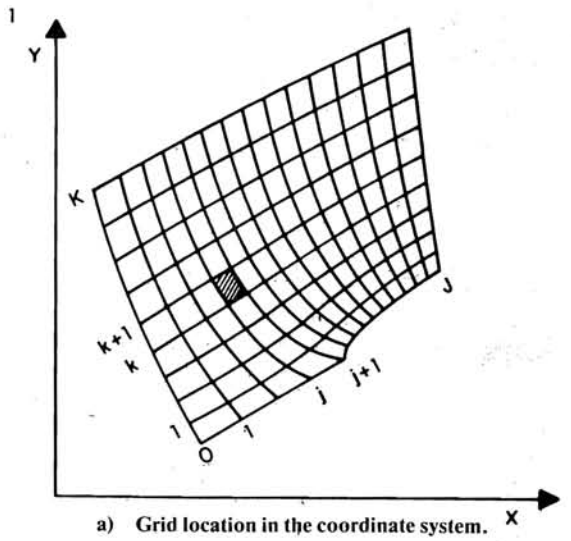


a) Grid location in the coordinate system.

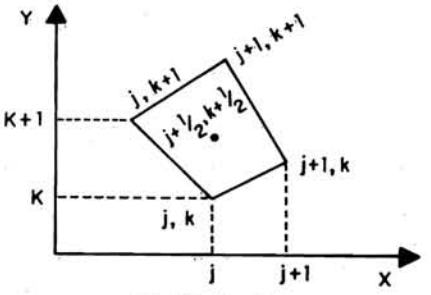


b) Single cell.

Fig. 2 Computational space notation.

#### Flow Periodicity Condition

By virture of the periodicity of the cascade flow over each interval of length $s$ in the $Y$ direction, the flow parameters over segments 1-3 and 5-7 in Fig. 1 are the same as those over 2-4 and 6-8, respectively. Hence, the segments 1-3, 5-7, 2-4, and 6-8 are essentially internal and there is no need to apply any boundary conditions to them. In the numerical solution, additional cells are attached to, but outside, these segments of the boundary. The flow parameters in the extra cells are set equal to the flow parameters in the corresponding cells inside the computational domain, which are displaced in the $Y$ direction by distance $s$.

The periodicity conditions are used only for cascade flow calculations.

## Numerical Solution

#### Godunov Method

Since the primary references of the multidimensional application of the Godunov method are not published in English, the method will be described here in some detail. The main idea of the Godunov method is to use the exact solution of the gasdynamic equations with piecewise constant initial conditions for the construction of the finite difference scheme.

It is assumed that a grid covers the computational domain as shown in Fig. 2a. We consider a fixed grid with the indexing of the lines as shown. The flow parameters in the center of the cell are given a fractional index: $j+\frac{1}{2},k+\frac{1}{2}$ (see Fig. 2b). The cell boundaries are given one fractional and one integer index: $j,k+\frac{1}{2}$ or $j+\frac{1}{2},k$. The parameters at the time $t$ are given a subscript index (i.e., $\rho_{j+\frac{1}{2},k+\frac{1}{2}}$) as distinct from the parameters at the time $t+\Delta t$, which are given a superscript index: $\rho^{j+\frac{1}{2},k+\frac{1}{2}}$.

With this notation, Eq. (1) is approximated to first-order accuracy by the following system of finite difference equations:

$$U^{j+\frac{1}{2},k+\frac{1}{2}} = U_{j+\frac{1}{2},k+\frac{1}{2}} - \frac{\Delta t}{\sigma_{j+\frac{1}{2},k+\frac{1}{2}}}$$

$$\times (\bar{F}_{j+\frac{1}{2},k}\Delta Y_{j+\frac{1}{2},k} - \bar{G}_{j+\frac{1}{2},k}\Delta X_{j+\frac{1}{2},k}$$

$$+\bar{F}_{j+1,k+\frac{1}{2}}\Delta Y_{j+1,k+\frac{1}{2}} - \bar{G}_{j+1,k+\frac{1}{2}}\Delta X_{j+1,k+\frac{1}{2}}$$

$$+\bar{F}_{j+\frac{1}{2},k+1}\Delta X_{j+\frac{1}{2},k+1} - \bar{G}_{j+\frac{1}{2},k+1}\Delta Y_{j+\frac{1}{2},k+1}$$

$$+\bar{F}_{j,k+\frac{1}{2}}\Delta X_{j,k+\frac{1}{2}} - \bar{G}_{j,k+\frac{1}{2}}\Delta Y_{j,k+\frac{1}{2}}) \qquad (2)$$

where $\sigma_{j+\frac{1}{2},k+\frac{1}{2}}$ is the area of the cell, and

$$\Delta Y_{j,k+\frac{1}{2}} = Y_{j,k+1} - Y_{j,k}$$

$$\Delta X_{j+\frac{1}{2},k} = X_{j+1,k} - X_{j,k}$$

$$U=\begin{vmatrix}\rho\\ \rho u\\ \rho v\\ e\end{vmatrix} \quad \bar{F}=\begin{vmatrix}RU\\ P+RU^2\\ RUV\\ (E+P)U\end{vmatrix} \quad \bar{G}=\begin{vmatrix}RV\\ RUV\\ P+RV^2\\ (E+P)V\end{vmatrix}$$

Here and in the following text we will denote with capital letters $R$, $U$, $V$, $P$, etc., the parameters at the edges of the cells. To obtain the values of the parameters at the edges we solve the Riemann problem with the initial left and right states given by those at the centers of the adjacent cells. The parameters $(R,U,V,P)_{j,k-\frac{1}{2}}$ are obtained from the solution of the one-dimensional Riemann problem[3] with the following initial conditions:

$$(\rho,W^n,P)_L = (\rho,W^n,P)_{j-\frac{1}{2},k-\frac{1}{2}} \quad \text{for} \quad X<X_j$$

$$(\rho,W^n,P)_R = (\rho,W^n,P)_{j+\frac{1}{2},k-\frac{1}{2}} \quad \text{for} \quad X>X_j \qquad (3)$$

where $W^n$ is the component of the velocity vector in the direction normal to the cell edge, here from $(j,k-1)$ to $(j,k)$. Subscripts $L$ and $R$ denote left and right states across a one-dimensional discontinuity. The solution of the Riemann problem with initial conditons given by Eq. (3) can be calculated using the algorithm described in Ref. 3. The parameters $(R,W^n,P)_{j,k-\frac{1}{2}}$ are the constant values that the solution gives at the point $(j,k-\frac{1}{2})$. The parameter $W^t_{j,k-\frac{1}{2}}$, which is the component of velocity parallel to the cell edge, is obtained as follows:

$$W^t_{j,k-\frac{1}{2}} = W^t_{j-\frac{1}{2},k-\frac{1}{2}}, \quad \text{if} \quad W^n_{j,k-\frac{1}{2}} > 0$$

$$= W^t_{j+\frac{1}{2},k-\frac{1}{2}}, \quad \text{if} \quad W^n_{j,k-\frac{1}{2}} \le 0$$

The values of $U_{j,k-\frac{1}{2}}$ and $V_{j,k-\frac{1}{2}}$ are then calculated from $W^n_{j,k-\frac{1}{2}}$ and $W^t_{j,k-\frac{1}{2}}$ using the unit normal of the cell edge. Similarly, the values of $(R,W^n,P)_{j-\frac{1}{2},k}$ are calculated as the solution of the Riemann problem at the point $j-\frac{1}{2},k$ with the following initial conditions across a discontinuity between $(j-\frac{1}{2},k-\frac{1}{2})$ and $(j-\frac{1}{2},k+\frac{1}{2})$:

$$(\rho,W^n,P)_L = (\rho,W^n,P)_{j-\frac{1}{2},k-\frac{1}{2}} \quad \text{for} \quad Y<Y_k$$

$$(\rho,W^n,P)_R = (\rho,W^n,P)_{j-\frac{1}{2},k+\frac{1}{2}} \quad \text{for} \quad Y>Y_k$$

The value of $W^t_{j-\frac{1}{2},k}$ is obtained from

$$W^t_{j-\frac{1}{2},k} = W^t_{j-\frac{1}{2},k-\frac{1}{2}}, \quad \text{if} \quad W^n_{j-\frac{1}{2},k} > 0$$

$$= W^t_{j-\frac{1}{2},k+\frac{1}{2}}, \quad \text{if} \quad W^n_{j-\frac{1}{2},k} \le 0$$

and the values of $U_{j-\frac{1}{2},k}$ and $V_{j-\frac{1}{2},k}$ are calculated from $W^n_{j-\frac{1}{2},k}$ and $W^t_{j-\frac{1}{2},k}$ using the unit normal of the cell edge.

The second-order method is constructed along lines similar to the first-order method. At each cell edge, the Riemann problem is solved for some specified pair of left and right states. The solution to this Riemann problem is then used in the calculation and differencing of numerical fluxes as above. The extension to second order is achieved by using extrapolation in space and time to obtain time-centered left and right limiting values as the input for the Riemann problem. Thus, the method described here is a natural extension of the one-dimensional method described in Ref. 6 to two dimensions, without the use of operator splitting in the coordinate directions.

In the following, we will give an outline of the main steps of the algorithm. Complete details and motivation are presented in Ref. 7.

In order to describe the idea behind this algorithm, we introduce a local coordinate transformation $(\xi,\eta) \leftrightarrow (x,y)$, such that, in terms of the new independent variables, Eqs. (1) are in the following form:

$$\frac{\partial JU}{\partial t} + \frac{\partial B_\xi}{\partial \xi} + \frac{\partial B_\eta}{\partial \eta} = 0 \qquad (4)$$

$$J = \mathrm{Det}\,[\nabla_{\xi,\eta}(x,y)]$$

$$B_\eta = \bar{n}_\eta \cdot (F,G) \qquad B_\xi = \bar{n}_\xi \cdot (F,G)$$

$$\bar{n}_\eta = \left(\frac{\partial y}{\partial \eta}, -\frac{\partial x}{\partial \eta}\right) \qquad \bar{n}_\xi = \left(-\frac{\partial y}{\partial \xi}, \frac{\partial x}{\partial \xi}\right)$$

where we have assumed $\partial x/\partial\xi, \partial y/\partial\eta > 0$.

We use the differential equation in this form to extrapolate in space and time the value of the solution centered at $(j-\frac{1}{2},k+\frac{1}{2},t^n)$ to $(j,k+\frac{1}{2},t^n+\Delta t/2)$, which we will take to be the left state for the Riemann problem at $(j,k+\frac{1}{2})$. Similarly, we extrapolate the value centered at $(j+\frac{1}{2},k+\frac{1}{2},t^n)$ to obtain the right state. The left and right states at $(j+\frac{1}{2},k)$ are obtained similarly. For example, $U_L$ and $U_R$, the left and right states at $(j,k+\frac{1}{2},t^n)$, are given by

$$U_{L,R} = U^n_{j-\frac{1}{2},k+\frac{1}{2}} + \frac{\Delta t}{2}\frac{\partial U}{\partial t} \pm \frac{\Delta\xi}{2}\frac{\partial U}{\partial \xi}$$

$$= U^n_{j-\frac{1}{2},k+\frac{1}{2}} - \frac{\Delta t}{2J}\left(\frac{\partial B_\xi}{\partial \xi} + \frac{\partial B_\eta}{\partial \eta}\right) \pm \frac{\Delta\xi}{2}\frac{\partial U}{\partial \xi}$$

$$= U^n_{j-\frac{1}{2},k+\frac{1}{2}} + \left(\pm\frac{\Delta\xi}{2} - \frac{\Delta t}{2J}A_\xi\right)\frac{\partial U}{\partial \xi}$$

$$+\left[-\frac{\Delta t}{2J}\frac{\partial \bar{n}_\eta}{\partial \xi}\cdot(F,G)\right] + \left(-\frac{\Delta t}{2J}\frac{\partial B_\eta}{\partial \eta}\right) \qquad (5)$$

where $\pm$ is assigned $(+,L)$, $(-,R)$. The last expression is obtained by putting $\partial B_\xi/\partial\xi$ in nonconservation form and rearranging terms, with $A_\xi$ the $4\times4$ matrix given by $A_\xi = \bar{n}_\eta \cdot (\nabla_U F, \nabla_U G)$.

To obtain an expression for $U_{L,R}$ computationally, we replace the spatial derivatives with finite differences. Some care is required in the choice of spatial differencing in order to obtain the monotone shock transitions without the introduction of artificial viscosity. In particular, $\partial U/\partial\xi$ is approximated by central differences, subject to monotonicity constraints, while $\partial B_\eta/\partial\eta$ is approximated by differencing first-order Godunov fluxes. For example, for the left state, the last three terms in Eq. (5) are approximated as follows:

$$\left(\pm\frac{\Delta\xi}{2}-\frac{\Delta t}{2J}A_\xi\right)\frac{\partial U}{\partial\xi}\approx\frac{1}{2}\Big\{1-\frac{\Delta t}{2\sigma_{j-\frac{1}{2},k+\frac{1}{2}}}$$

$$\times[(\Delta Y_{j-\frac{1}{2},k+1}+\Delta Y_{j-\frac{1}{2},k})(\nabla_U F)(U_{j-\frac{1}{2},k+\frac{1}{2}})$$

$$-(\Delta X_{j-\frac{1}{2},k+1}+\Delta X_{j-\frac{1}{2},k})(\nabla_U G)(U_{j-\frac{1}{2},k+\frac{1}{2}})]\Big\}\delta U_{j-\frac{1}{2},k+\frac{1}{2}} \quad (6a)$$

$$\left[-\frac{\Delta t}{2J}\frac{\partial\bar{n}_\eta}{\partial\xi}\cdot(F,G)\right]\approx-\frac{\Delta t}{2\sigma_{j-\frac{1}{2},k+\frac{1}{2}}}$$

$$\times[(\Delta Y_{j,k+\frac{1}{2}}-\Delta Y_{j-1,k+\frac{1}{2}})F(U_{j-\frac{1}{2},k+\frac{1}{2}})$$

$$-(\Delta X_{j,k+\frac{1}{2}}-\Delta X_{j-1,k+\frac{1}{2}})G(U_{j-\frac{1}{2},k+\frac{1}{2}})] \quad (6b)$$

$$\left(-\frac{\Delta t}{2J}\frac{\partial B_\eta}{\partial\eta}\right)\approx-\frac{\Delta t}{2\sigma_{j-\frac{1}{2},k+\frac{1}{2}}}$$

$$\times\{-[\Delta Y_{j+\frac{1}{2},k+1}F(U^l_{j+\frac{1}{2},k+1})-\Delta Y_{j+\frac{1}{2},k}F(U^l_{j+\frac{1}{2},k})]$$

$$+[\Delta X_{j+\frac{1}{2},k+1}G(U^l_{j+\frac{1}{2},k+1})-\Delta X_{j+\frac{1}{2},k}G(U^l_{k+\frac{1}{2},k})]\} \quad (6c)$$

In smooth regions, $\delta U_{j-\frac{1}{2},k+\frac{1}{2}}$ is a central difference of $U$ in the $j$ direction, e.g., $\delta U_{j-\frac{1}{2},k+\frac{1}{2}}=\frac{1}{2}(U_{j+\frac{1}{2},k+\frac{1}{2}}-U_{j-3/2,k+\frac{1}{2}})$, which is subject to certain monotonicity constraints at discontinuities. The values $U^l_{j+\frac{1}{2},k+1}$ are obtained by solving the Riemann problem at $(j+\frac{1}{2},k+1)$ using the piecewise constant states as described above for the Godunov method.

There are a number of details of the implementation omitted here. For example, we do not include all of the corrections represented by Eq. (6b) to $U_{j-\frac{1}{2},k+\frac{1}{2}}$, but rather include only those components in an expansion in terms of characteristic vectors of $A_\xi$ corresponding to waves approaching $(j,k+\frac{1}{2})$. Also, we perform the correction in terms of the primitive variables $p$, $\rho$, $u$, and $v$ rather than the conserved quantities. Finally, we use a more elaborate interpolation and monotonicity criteria than the central difference algorithm used in Ref. 1.

## Results and Discussion

The two numerical methods described in the previous section were combined into a single code in such a way that we could readily select between one method or the other in solving a specified flow problem. This could be done very easily since the two methods differ structurally only in the algorithms used to define the left and right states in the elemental Riemann problem. The second-order method has more computational steps per iteration and is therefore more demanding of machine time. For this reason, to obtain steady-state solutions with the second-order method, it is practical first to use the cheaper Godunov method for several hundred iterations.

The problem of the flow in a channel with a circular arc "bump" was chosen to evaluate the code for subsonic, transonic, and supersonic steady-state modeling. This particular problem is well suited for code development and testing. The geometry and the grids are easy to generate accurately and the problem symmetry and geometrical simplicity aid the interpretation of the results. Two circular arc bump thickness-to-chord ratios were used: 10% for subsonic and transonic modeling, 4% for the supersonic model. To the upper and lower boundaries of the channel, the solid-wall boundary condition was applied. The inflow boundary is on the left side.

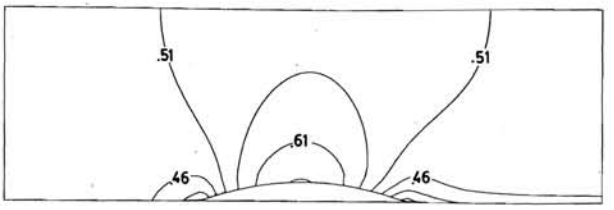


Fig. 3 Isomach lines, Godunov method.

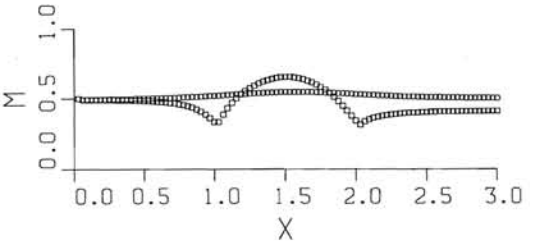


a) Godunov method.

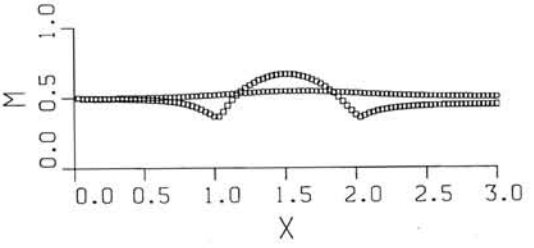


b) Godunov method rounded corners.

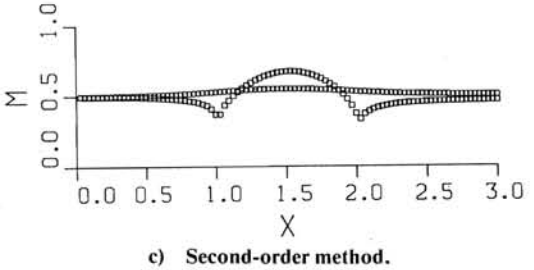


c) Second-order method.

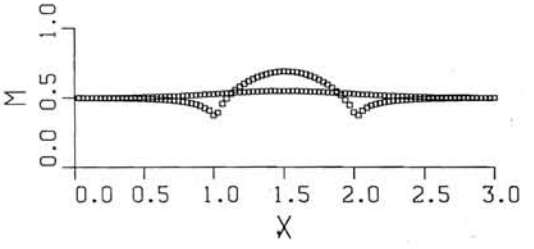


d) Second-order method, boundary conditions as in Ref. 8.

Fig. 4 Surface Mach number for flow in the channel at $M_{-\infty}=0.5$.

Figure 3 shows isomach lines of the steady flow solution for an upstream Mach number, $M_{-\infty}=0.5$, obtained using the Godunov method. A noticeable asymmetry is seen in the solution. A small "horseshoe-like" vortex sheet is attached to the trailing edge of the bump.

On investigation, it was found that vorticity is introduced at sharp leading and trailing edges where there is a discontinuous change in the streamline slope. The results in Figs. 4a and 4b demonstrate how very slight changes in the coordinates in the regions of the leading and trailing edges influence the

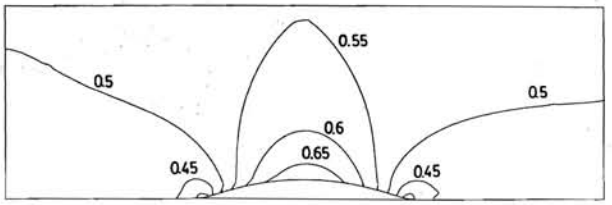


Fig. 5 Isomach line, second-order method.

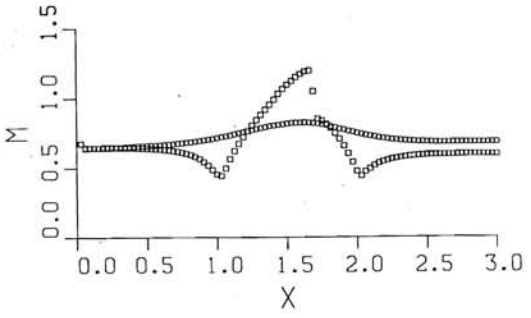


a) Godunov method.

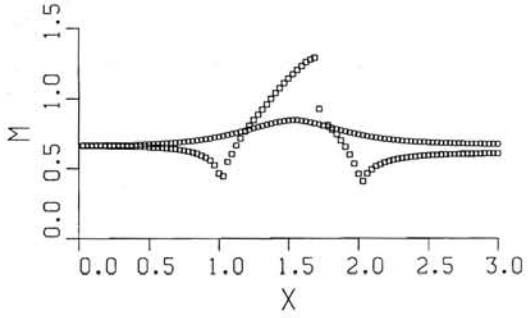


b) Second-order method.

Fig. 6 Surface Mach number for flow in the channel at $M_{-\infty} = 0.675$.

distribution of the Mach number over the surface. Figure 4a shows the solution using the original grid. In Fig. 4b the solution is shown for a grid where the one wall point just ahead of the corner was lifted 0.0005 and the corner point was lifted 0.0015, expressed as a fraction of the chord length. A symmetrical change was made to the corner point and the point just behind it at the trailing edge.

The asymmetry of the flow and pressure losses at the corner could be reduced further by special numerical treatment of the corner points, such as extrapolation of the values at the corners from the flowfield values.

Figure 4c shows the surface Mach number distribution for the same test case, calculated using the second-order extension of the Godunov method. It can be seen that the use of the higher-order accurate method leads to a significant improvement of the results; the symmetry in Fig. 4c is considered to be very good.

In all of the cases with subsonic flow over the 10% arc bump described above, the solution of the Riemann problem was used to determine the fluxes of conserved quantities at the boundary. In order to check how the particular definition of a solid-wall boundary adopted in Ref. 8 would influence the solution, we implemented with the second-order method such an iterative routine to satisfy normal momentum, streamwise momentum, and flow tangency. The results are shown in Figs. 4d and 5.

Here we see further improvement in the symmetry. However, this boundary condition was not adopted or used in

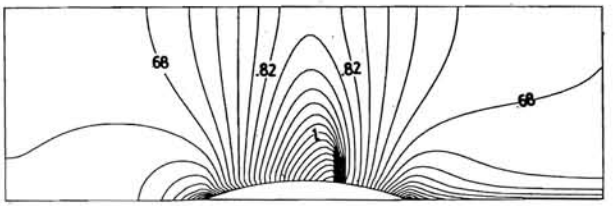


a) Godunov method.

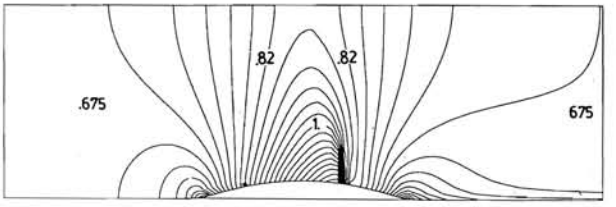


b) Second-order method.

Fig. 7 Isomach line for transonic flow in the channel, $M_{-\infty} = 0.675$.

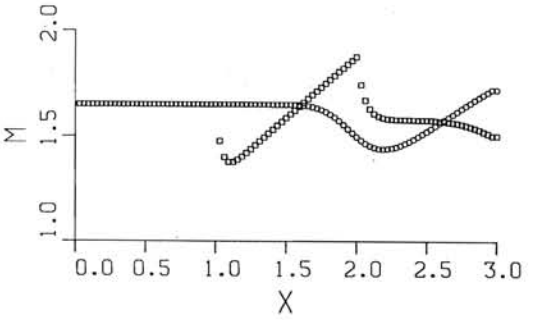


a) Surface Mach numbers.

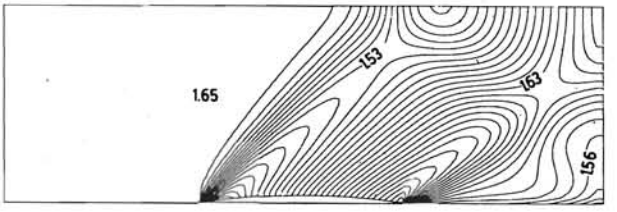


b) Isomach lines.

Fig. 8 Supersonic solution for flow in channel with 4% thick circular arc bump, $M_{-\infty} = 1.65$, Godunov method.

all of the other results reported in this study. The reason is that the code is intended to be used for nonsteady transonic flows and the theoretical ground for using this kind of boundary routine is not clear in such cases.

Figures 6 and 7 present the Mach number distribution and isomach lines of the transonic flow solution for the same 10% thick arc bump for $M_{-\infty} = 0.675$ using the Godunov method and its second-order extension, respectively. Comparison of the two figures shows that there is a sharper shock in the case of the second-order method—the maximum value in this case is 10% higher than in the Godunov method. The shock is located at a distance of 72% of the chord and the maximum value of the Mach number is 1.32 in case of the higher-order calculations. This agrees closely with the values obtained by Ni[9] for the same problem.

Figures 8 and 9 present results for the supersonic flow in a channel with a 4% thick arc bump for $M_{-\infty} = 1.65$ obtained

**Table 1 Design data for Sanz compressor cascade**

| | |
|---|---|
| Inlet Mach number $M_{-\infty}$ | 0.713 |
| Inlet flow angle $\alpha$ | 31.58 deg |
| Outlet Mach number $M_{+\infty}$ | 0.57 |
| Outlet flow angle $\beta$ | 1.3 deg |
| Blade gap/chord ratio | 1.306 |

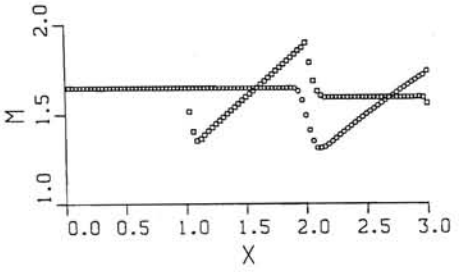


a) Surface Mach number.

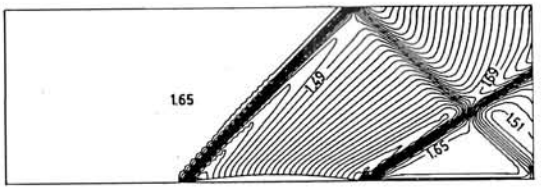


b) Isomach lines.

**Fig. 9 Supersonic solution for flow in a channel with a 4% thick circular arc bump, $M_{-\infty} = 1.65$, second-order method.**

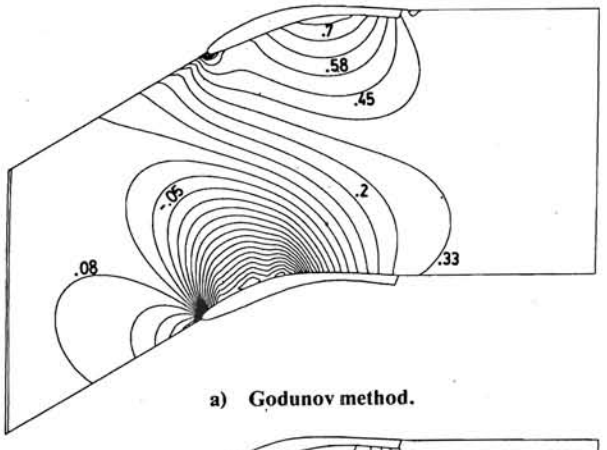


a) Godunov method.

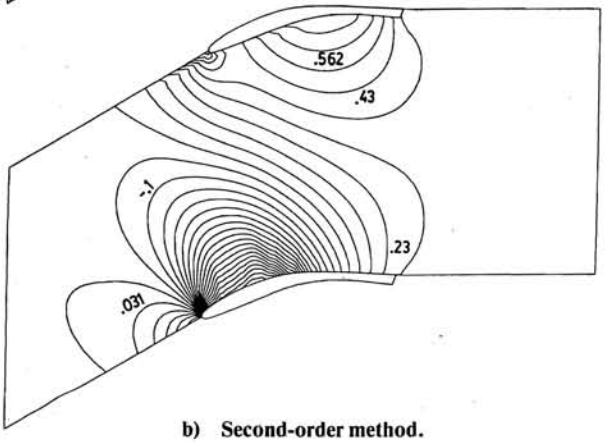


b) Second-order method.

**Fig. 10 Isobar lines ($C_p$) for the Sanz supercritical cascade.**

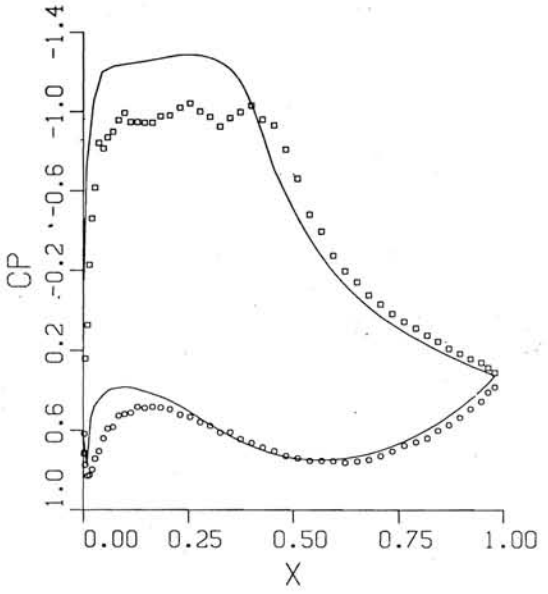


a) Godunov method.

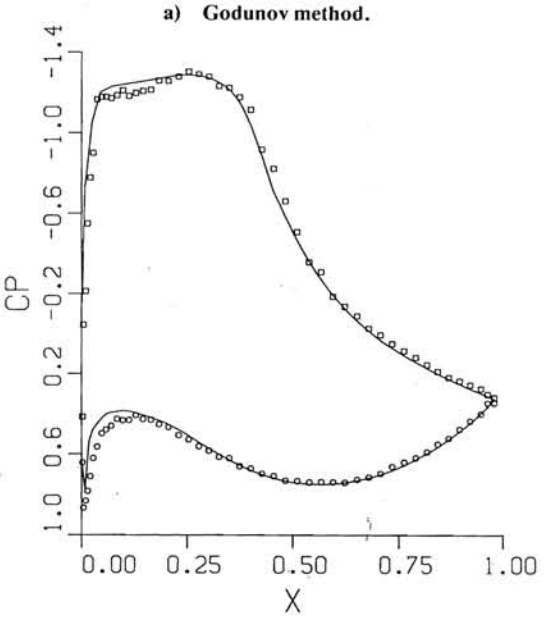


b) Second-order method.

**Fig. 11 Surface pressure coefficient $C_p$ distribution for the Sanz cascade (continuous lines show reference $C_p$ distribution).**

with the Godunov method and the second-order method, respectively. Although the general behavior of the two solutions is seen to be similar, the more accurate description of shock waves obtainable with the higher-order method resulted in better resolution of the complex shock structure, of which the basic Godunov method gave only a vague picture.

The ability of the code to model turbomachinery cascade flows was tested first using a shockless supercritical compressor cascade designed by Sanz.[10] The design data for the cascade are listed in Table 1. Figure 1 shows the mesh that was used to calculate the flow through the Sanz cascade. The mesh was generated using the code described in Ref. 11. The attempt was made to calculate as closely as possible the original design problem. The blade trailing edge was not changed geometrically and a symmetry boundary condition was imposed between the one point on the trailing edge and the last point on the suction side of the profile. The mesh was $89 \times 33$ with 48 points on the profile.

In Fig. 10 are shown the isobars (of constant pressure coefficient $C_p$) for the flow in the Sanz cascade calculated

using the Godunov method (Fig. 10a) and the second-order method (Fig. 10b). The pseudoviscous effect resulting from large truncational errors in the Godunov method leads to a partial blockage of the outlet flowfield and does not allow the design inlet flow velocity to be reached. As it can be seen in Fig. 10a, partial blockage of the flow results in jump-like changes in the pressure coefficient at the inlet from the imposed design conditions to those calculated in the solution. In contrast, in Fig. 10b the design boundary conditions are reached at steady state using the second-order extension of the Godunov method, which has a significantly lower truncational error.

In Fig. 11 the design pressure coefficient distribution over the cascade blade surface[10] is compared with that calculated using the Godunov and second-order methods, respectively. The basic Godunov method is seen to give a maximum error of $\approx 30\%$ in the supersonic region, while the second-order extension of the Godunov method gives $C_p$ values that correspond very well to the design conditions specified by Sanz.[10]

The Godunov method exhibited faster convergence to the steady state than the second-order method because of the increased damping associated with the larger truncational error. For the case of subsonic flow over the 10% circular arc bump, which was calculated using a $99 \times 33$ grid, convergence was obtained for the Godunov method in approximately 1200 iterations, approximately half the number required for the second-order method. No attempt has yet been made to optimize the code. More detailed investigations of the convergence of the methods will be made as the efficiency of the code is improved. The second-order code takes $\approx 3$ times more CPU time per iteration than the Godunov method. An extensive comparison of the computational efficiency for the Godunov, MacCormack, and second-order Godunov codes is given in Ref. 2.

## Conclusion

A comparison of the performance of the Godunov method and a newly developed second-order extension of the method in calculating steady two-dimensional internal flows showed that the second-order method significantly improved the accuracy of the solution (by reducing numerical dissipation), while it retained the robustness inherent in the Godunov technique. The second-order method was found to describe shock waves very accurately, with minimal shock dissipation over the computational mesh. Therefore, the method has significant potential for the computation of complex transonic and supersonic flowfields.

The first applications using the second-order method to calculate comparatively low Mach numbers and shock-free internal transonic flows using nonorthogonal and nonuniform grids were also successful. In particular, the present code was shown to give good agreement with design data for a Sanz supercritical compressor cascade. No changes to the code were required for computing the particular Mach number. Thus, design and off-design flow conditions for a particular cascade geometry can now be obtained easily.

The computational efficiency of the code has not yet been established, since no attempt was made to optimize in the process of early development. Nevertheless, it is clear that calculations with the second-order method are likely to be more expensive than with currently accepted methods (e.g., MacCormack). Use of the method would be justified, however, for calculating complex flow structures involving shock waves and for modeling unsteady supersonic and transonic flows.

## Acknowledgments

The authors gratefully acknowledge the participation of Dr. R. Mendez and are indebted to Dr. J. Sanz of NASA Lewis Research Center for supplying the supercritical cascade data and also to Professor R. Camarero of Ecole Polytechnique, Montreal, for supplying the grid generation routine. The study was initiated and performed largely while the first author was an NRC Research Associate at the Naval Postgraduate School. Acknowledgment is made for support received under this program. The second author was supported by the U.S. Department of Energy and the U.S. Defense Nuclear Agency.

## References

[1] Van Leer, B., "Towards the Ultimate Conservative Difference Scheme," *Journal of Computational Physics*, Vol. 32, 1979, pp. 101-136.

[2] Woodward, P. and Colella, P., "The Numerical Simulation of Two-Dimensional Fluid Flow with Strong Shock," *Journal of Computational Physics*, to be published.

[3] Godunov, S. K. et al., "Numerical Solution of Multidimensional Problems in Gas Dynamics," Nauka, Moscow, 1976 (in Russian).

[4] Sod, G. A., "A Survey of Several Finite Difference Methods for Systems of Nonlinear Hyperbolic Conservation Laws," *Journal of Computational Physics*, Vol. 27, 1978, pp. 1-31.

[5] Thompkins, W. T. Jr. and Tong, S. S., "Inverse or Design Calculation for Non-Potential Flow in Turbomachinery Blade Passages," ASME Paper 81-GT-78, 1981.

[6] Colella, P. and Woodward, P. R., "The Piecewise-Parabolic Method (PRM) for Gas-Dynamical Simulations," *Journal of Computational Physics*, to be published.

[7] Colella, P., "A Multidimensional Second-Order Godunov Method for Hyperbolic Conservation Laws," Lawrence Berkeley Laboratory, Berkeley, Calif., Rept. LBL-17023, Dec. 1983.

[8] Thompkins, W. T. Jr., Tong, S. S., Bush, R. H., Usab, W. J. Jr., and Norton, R. J. G., "Solution Procedures for Accurate Numerical Simulation of Flow in Turbomachinery Cascades," AIAA Paper 83-0257, Jan. 1983.

[9] Ni, R. H., "A Multiple-Grid Scheme for Solving the Euler Equations," *AIAA Journal*, Vol. 20, Nov. 1982, pp. 1565-1571.

[10] Sanz, J. M., Private communication, Jan. 1983.

[11] Camarero, R. and Younist, M., "Efficient Generation of Body-Fitted Coordinates for Cascade Using Multigrid," *AIAA Journal*, Vol. 18, May 1980, pp. 487-488.